Provided for non-commercial research and education use.
Not for reproduction, distribution or commercial use.

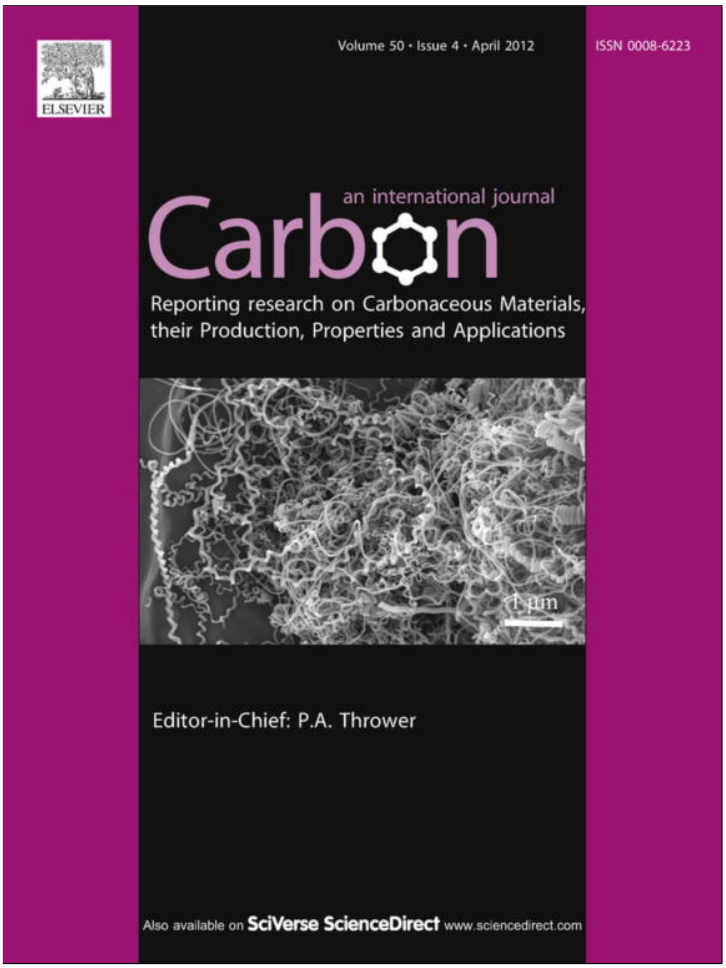

This article appeared in a journal published by Elsevier. The attached copy is furnished to the author for internal non-commercial research and education use, including for instruction at the authors institution and sharing with colleagues.

Other uses, including reproduction and distribution, or selling or licensing copies, or posting to personal, institutional or third party websites are prohibited.

In most cases authors are permitted to post their version of the article (e.g. in Word or Tex form) to their personal website or institutional repository. Authors requiring further information regarding Elsevier's archiving and manuscript policies are encouraged to visit:

http://www.elsevier.com/copyright

Author's personal copy

CARBON 50 (2012) 1583–1590

Available at www.sciencedirect.com

SciVerse ScienceDirect

journal homepage: www.elsevier.com/locate/carbon

Quenched solid density functional theory method for characterization of mesoporous carbons by nitrogen adsorption

Gennady Yu. Gor [a,1], *Matthias Thommes* [b], *Katie A. Cychosz* [b], *Alexander V. Neimark* [a,*]

[a] *Rutgers University, Department of Chemical and Biochemical Engineering, 98 Brett Road, Piscataway, NJ 08854, USA*
[b] *Quantachrome Instruments, Boynton Beach, FL 33426, USA*

ARTICLE INFO

Article history:
Received 1 August 2011
Accepted 23 November 2011
Available online 29 November 2011

ABSTRACT

Quenched solid density functional theory (QSDFT) model for characterization of mesoporous carbons using nitrogen adsorption is extended to cylindrical and spherical pore geometries. The kernels of theoretical isotherms in the range from 0.4 to 50 nm are constructed accounting for different possible variations of the pore shapes in micropore and mesopore regions. The results of QSDFT method are illustrated with experimental data on adsorption on novel CMK-3 and 3DOm carbons. The proposed method is recommended for pore size distribution calculations for micro–mesoporous carbons obtained through various templating mechanisms.

© 2011 Elsevier Ltd. All rights reserved.

1. Introduction

The application of the non-local density functional theory (NLDFT) method to gas adsorption data has led to major advances in the textural characterization of porous materials. NLDFT methods allow one to describe the adsorption and phase behavior in fluids on the molecular level [1–3] and to obtain pore size information over the complete range of micro- and mesopores [4–9].

A comprehensive library of NLDFT methods for the interpretation of experimental data and calculation of pore size distributions (PSDs) for various types of materials has been implemented in the data reduction software of commercial instruments, which are currently widely used for structure characterization of various mesoporous and microporous materials based on adsorption of nitrogen, argon, and carbon dioxide. As such, the NLDFT method is now commonly applied and it is featured in a recent standard by ISO [10].

While NLDFT has been demonstrated to be a reliable method for characterization of a variety of ordered and hierarchically structured materials, a drawback of the standard NLDFT methods is that they do not take into account chemical and geometrical heterogeneity of the pore walls, assuming a structureless, chemically and geometrically smooth surface model. The consequence of this mismatch between the theoretical assumption of a smooth and homogeneous surface and the real molecularly heterogeneous surfaces of porous solids is that the theoretical NLDFT adsorption isotherms exhibit multiple steps associated with layering transitions related to the formation of a monolayer, second adsorbed layer, and so on. The problem is enhanced in many porous carbon materials, which exhibit (in contrast to micro and mesoporous zeolites and mesoporous molecular sieves for instance) broad PSDs, where artificial layering steps inherent to the theoretical isotherms cause artificial gaps on the calculated pore size distributions. Recently, the NLDFT method was advanced to take into account the molecular level surface roughness that is typical to most carbonaceous, siliceous, and other materials, including hybrid organic–inorganic hierarchical structures [3]. This technique, named

* *Corresponding author.*
E-mail addresses: ggor@princeton.edu (G.Y. Gor), aneimark@rci.rutgers.edu (A.V. Neimark).
[1] Current address: Department of Civil and Environmental Engineering, Princeton University, Princeton, NJ 08544, USA.
0008-6223/$ - see front matter © 2011 Elsevier Ltd. All rights reserved.
doi:10.1016/j.carbon.2011.11.037

Author's personal copy

the quenched solid density functional theory (QSDFT), was shown to be more reliable then NLDFT for analyses of microporous carbons [11].

The QSDFT method for carbons [11] has been originally developed assuming slit-shaped pores, which are typical model pores in activated microporous carbons. However, the emergence of novel materials with pre-designed pore morphology (obtained by synthesis routes, which make use of structure directing agents or hard templates) requires the development of new methods, which take into account the morphological specifics of these structures. The current work extends the QSDFT method to micro–mesoporous carbons with cage-like and channel-like pore geometries. To this end, we have built a set of hybrid QSDFT kernels comprising of the theoretical isotherms of nitrogen adsorption in spherical and cylindrical pores ranging from 0.4 to 50 nm embracing the whole range of micro- and mesopores. The application of the proposed QSDFT kernels is demonstrated on two examples of novel micro–mesoporous carbons possessing either cylindrical or spherical mesopores. First, we consider nitrogen adsorption on CMK-3 carbons – two-dimensional hexagonally ordered materials obtained as carbon inverse replicas from the SBA-15 silica templates [12]. The second system is three-dimensionally ordered mesoporous (3DOm) carbons, synthesized by templating three-dimensional colloidal crystals formed from lysine-silica nanoparticles [13]. The pore size distributions obtained using the proposed kernels are compared with the X-ray diffraction (XRD) analysis of CMK-3 sample and with scanning electron microscopy (SEM) data of 3DOm carbon samples.

2. Method

To develop a new DFT method for a given class of porous materials, one needs to calculate a set of theoretical adsorption isotherms for the wide range of pore sizes, called the kernel, taking into account the specifics of the pore geometry and the parameters of adsorbate–adsorbate and adsorbate–adsorbent interactions. The PSD is derived by means of solution of the integral adsorption equation, which presents the experimental isotherm as the convolution of the DFT kernel of theoretical isotherms [14].

2.1. QSDFT approach

The process of adsorption in a pore is usually treated within a grand canonical ensemble, at given temperature and adsorbate chemical potential, therefore the conditions of adsorption equilibrium are determined by the grand thermodynamic potential of the adsorption system presented as a functional of the fluid density. Conventionally in NLDFT [15,16] the grand thermodynamic potential of fluid Ω_f is considered, while the role of solid is displayed only through an external potential U_{ext},

$$\Omega_f[\rho_f(\mathbf{r})] = F_f[\rho_f(\mathbf{r})] - \int d\mathbf{r}\rho_f(\mathbf{r})[\mu_f - U_{ext}(\mathbf{r})]. \quad (1)$$

Here $\mathbf{r}$ is a position vector, $\rho_f(\mathbf{r})$ is the fluid density profile, μ_f is the chemical potential of the fluid, F_f is the Helmholtz free energy of the fluid. The latter is expressed as a sum of the ideal term $F_{id}[\rho_f(\mathbf{r})]$, excess hard-sphere repulsion term $F_{ex}[\rho_f(\mathbf{r})]$ and attractive term calculated in a mean-field fashion,

$$F_f\left[\rho_f(\mathbf{r})\right] = \mathbf{F}_{id}\left[\rho_f(\mathbf{r})\right] + F_{ex}\left[\rho_f(\mathbf{r})\right] + \frac{1}{2}\int\int d\mathbf{r}d\mathbf{r}'\rho_f(r)\rho_f(r')u_{ff}(|\mathbf{r}-\mathbf{r}'|) \quad (2)$$

where $u_{ff}(r)$ is the attractive part of fluid–fluid potential. The fluid density profile $\rho_f(\mathbf{r})$ is obtained from minimization of the grand potential (1). For the details of conventional NLDFT approach see the review [17].

As it was mentioned above, since within the NLDFT model the solid surface is treated as molecularly smooth, its predictions imply pronounced layering steps on adsorption isotherms, which are not displayed by experimental adsorption isotherms on amorphous and semi-crystalline materials, like carbons and silica. This drawback is overcome in the QSDFT model, which accounts for the surface roughness effects [3,11].

Within the framework of QSDFT, the grand potential of both solid and fluid are considered. As such, QSDFT, unlike conventional NLDFT, implies a two-component density functional, where the solid is modeled as a compound of hardcore spheres, interacting with the fluid molecules via a pairwise attractive potential. Likewise Eqs. (1) and (2), the grand potential of the solid–fluid system Ω_{sf} is written as

$$\begin{aligned}\Omega_{sf}[\rho_s(\mathbf{r}),\rho_f(\mathbf{r})] = {} & F_{id}[\rho_f(\mathbf{r})] + F_{id}[\rho_s(\mathbf{r})] + F_{ex}[\rho_f(\mathbf{r}),\rho_f(\mathbf{r})] \\ & + \frac{1}{2}\int\int d\mathbf{r}d\mathbf{r}'\rho_f(\mathbf{r})\rho_f(\mathbf{r}')u_{ff}(|\mathbf{r}-\mathbf{r}'|) \\ & + \frac{1}{2}\int\int d\mathbf{r}d\mathbf{r}'\rho_s(\mathbf{r})\rho_s(\mathbf{r}')u_{ss}(|\mathbf{r}-\mathbf{r}'|) \\ & + \int\int d\mathbf{r}d\mathbf{r}'\rho_f(\mathbf{r})\rho_s(\mathbf{r}')u_{sf}(|\mathbf{r}-\mathbf{r}'|) \\ & - \mu_f\int d\mathbf{r}\rho_f(\mathbf{r}) - \mu_s\int d\mathbf{r}\rho_s(\mathbf{r}) \end{aligned} \quad (3)$$

where $\rho_s(\mathbf{r})$ is the density profile of the solid component, $F_{id}[\rho_s(\mathbf{r})]$ is the ideal contribution of hard-sphere free energy of the solid, $F_{ex}[\rho_s(\mathbf{r}),\rho_f(\mathbf{r})]$ is the excess hard sphere free energy term for both solid and liquid components, $u_{ss}(r)$, $u_{sf}(r)$ are the attractive parts of solid–solid and solid–fluid potentials, μ_s is the chemical potential of the solid. The key term of QSDFT approach in Eq. (3) is $F_{ex}[\rho_s(\mathbf{r}),\rho_f(\mathbf{r})]$ – the excess free energy of the solid–fluid hard spheres mixture. To calculate this term we employ Rosenfeld's fundamental measure theory [18,19], which is consistent with the Percus–Yevick equation of state for bulk hard spheres fluid (see details in [11]).

A significant simplification, which saves much computation time, is related to the "quenched" state of the solid: while we take into account the density of the solid component $\rho_s(\mathbf{r})$, we do not vary it while optimizing the grand potential Ω_{sf}. Thus only those terms, which are related to the fluid in Eq. (3) are subject to minimization. The final density profile is found from the condition

$$\left.\frac{\delta\Omega[\rho_s(\mathbf{r}),\rho_f(\mathbf{r})]}{\delta\rho_f(\mathbf{r})}\right|_{\rho_s(\mathbf{r})} = 0, \quad (4)$$

which leads to the solution of the Euler–Lagrange equation

$$\begin{aligned}\rho_f(\mathbf{r}) = \Lambda_f^{-3}\exp\Big\{ & c^{(1)}(\mathbf{r},[\rho_s,\rho_f]) - \beta\int d\mathbf{r}'\rho_f(\mathbf{r})u_{ff}(|\mathbf{r}-\mathbf{r}'|) + \beta\mu_f \\ & - \beta\int d\mathbf{r}'\rho_s(\mathbf{r})u_{sf}(|\mathbf{r}-\mathbf{r}'|)\Big\} \end{aligned} \quad (5)$$

Author's personal copy

where $c^{(1)}(\mathbf{r},[\rho_s,\rho_f]) = -\beta\delta F_{ex}[\rho_s(\mathbf{r}),\rho_f(\mathbf{r})]/\delta\rho_f(\mathbf{r})$ depends on both solid and fluid densities. Here $\beta = 1/k_BT$, k_B is the Boltzmann constant, T is the absolute temperature, $\Lambda_f = h/(2\pi mkT)^{1/2}$ is the thermal de Broigle wavelength, h is the Planck constant, and m is the mass of the fluid molecule.

2.2. Parameters of the model

We use the same parameters for solid and fluid as were used in the preceding work [11], based on the experiments on nitrogen adsorption on Cabot BP-280 carbon. Both fluid–fluid and solid–fluid molecular interactions parameters are presented as Lennard–Jones potentials with the following parameters: $\varepsilon_{ff}/k_B = 95.77$ K, $\sigma_{ff} = d_{HS} = 0.3549$ nm and $\varepsilon_{sf}/k_B = 150$ K, $\sigma_{sf} = 0.269$ nm.

Similarly to the QSDFT model [11], the "quenched" profile of the solid density as a one-dimensional function represents the linear ramp and is given by the relation:

$$\rho_s(z) = \begin{cases} \rho_s^0 & 0 \le z < h_0 \\ 0.75\rho_s^0\left(1 - \frac{z-h_0}{2\delta}\right) & h_0 \le z < h_0 + 2\delta \\ 0 & h_0 + 2\delta \le z \end{cases} \quad (6)$$

Here $\rho_s^0 = 1.14 \times 10^{29}$ m^{-3} is the bulk density of carbon, $h_0 = 2 \times 0.34$ nm is the thickness of the solid wall, and $\delta = 0.13$ nm is the roughness parameter, the origin of z coordinate is on the edge of the pore. The value of roughness parameter corresponds to the reference nitrogen isotherm on a sample of Cabot BP-280 carbon black with a partial degree of graphitization [11]. The hard sphere diameter of the carbon atoms is 0.2217 nm. Position of the edge of the solid, which is responsible for the pore size D discussed in Section 2.3 is determined from the condition of zero solid excess.

2.3. Recovering the pore size distribution using QSDFT

PSD is calculated from the experimental adsorption isotherm $N_{exp}(P/P_0)$ by solution of the integral adsorption equation. The experimental isotherm is represented as the convolution of the QSDFT kernel (set of the theoretical isotherms $N_{QSDFT}(P/P_0, D)$ in a series of pores within a given range of pore sizes D) and the sought PSD function $f(D)$,

$$N_{exp}(P/P_0) = \int_{D_{min}}^{D_{max}} N_{QSDFT}(P/P_0, D) f(D) dD. \quad (7)$$

Here D_{min} and D_{max} are the minimum and maximum pore sizes in the kernel. The kernel of selected QSDFT adsorption isotherms for the cylindrical geometry is presented in Fig. 1. In contrast to the NLDFT kernels, the QSDFT isotherms are smooth prior the capillary condensation steps, which are characteristic to mesopores ($D > 2$ nm), and do not exhibit stepwise inflections caused by artificial layering transitions.

Solution of Eq. (8) can be obtained using the quick non-negative least square method [20]. In this method Eq. (8) is represented as a matrix equation, which is solved using the discrete Tikhonov regularization method combined with the non-negative least square algorithm [21].

3. Kernels of theoretical adsorption isotherms for characterization of micro–mesoporous carbons

The isotherms of nitrogen adsorption were calculated for slit, cylindrical, spherical carbon pores in the whole range of pore sizes, which can be probed in high resolution adsorption measurements with the lowest relative pressure $P/P_0 = 10^{-9}$. While the isotherms in micropores are equilibrium and reversible, the adsorption and desorption isotherms in

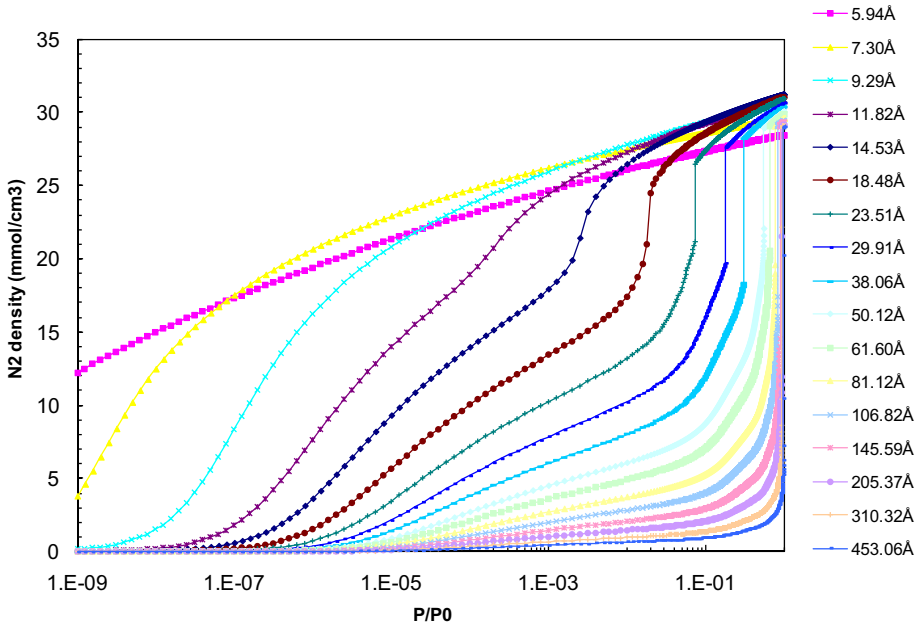

Fig. 1 – Kernel of selected metastable adsorption isotherms of nitrogen at 77.4 K in cylindrical pores with molecularly rough walls using the surface model for Cabot BP-280 carbon black. The pore widths are given in the right panel.

Author's personal copy

mesopores exhibit hysteresis. As such, different kernels are required for calculating PSD from adsorption and desorption branches of experimental isotherms.

For PSD calculations in micro–mesoporous carbons with various characteristic shapes of micro- and mesopores, we constructed six different kernels, each composed of 134 QSDFT theoretical adsorption isotherms:

(1) Kernel of equilibrium isotherms in cylindrical pores ranging from 0.5175 to 50.2 nm, called below the cylindrical equilibrium kernel.
(2) Kernel of metastable adsorption isotherms in cylindrical pores ranging from 5.01 to 50.2 nm, and equilibrium isotherms in cylindrical pores ranging from 0.5175 to 4.84 nm, called below the cylindrical adsorption kernel.
(3) Hybrid kernel composed of equilibrium isotherms in cylindrical mesopores ranging from 2.12 to 50.2 nm and in slit-shaped micropores ranging from 0.375 to 2.0 nm, called below the hybrid slit-cylindrical equilibrium kernel.
(4) Hybrid kernel of metastable adsorption isotherms in cylindrical mesopores ranging from 5.01 to 50.2 nm, equilibrium isotherms in cylindrical mesopores ranging from 2.12 to 50.2 nm, and equilibrium isotherms in slit-shaped micropores ranging from 0.375 to 2.0 nm, called below the slit-cylindrical adsorption kernel.
(5) Hybrid kernel composed of metastable adsorption isotherms in spherical mesopores ranging from 5.01 to 50.2 nm and equilibrium isotherms in cylindrical meso- and micropores ranging from 0.5175 to 4.84 nm, called below the cylindrical-spherical adsorption kernel.
(6) Hybrid kernel composed of metastable adsorption isotherms in spherical mesopores ranging from 5.01 to 50.2 nm, equilibrium isotherms in cylindrical mesopores ranging from 2.12 to 4.84 nm, and equilibrium isotherms in slit-shaped micropores ranging from 0.375 to 2.0 nm, called below the slit-cylindrical-spherical adsorption kernel.

The constructed kernels reflect a variety of possible characteristic morphologies in micro–mesoporous carbon, which are reflected in the shape and type of the hysteresis loop formed by adsorption and desorption branches. Kernels 1–4 are designed for materials, in which the mesopore system is comprised either of an array or a 3D network of channels of quasi-cylindrical shape, such as carbons prepared from hexagonally ordered templates, like CMK-3 [12], CMK-5 [22], MWCMK-3 [23], etc. Kernels 1 and 3 can be recommended for pore size analysis from either the reversible experimental isotherm, or from the desorption branch of the hysteretic isotherm of type H1. Kernels 2 and 4 can be recommended for treating the adsorption branch of the hysteretic isotherm of H2 type. Kernels 3 and 4 would be more suitable for samples with a substantial degree of activation that leads to the formation of slit-shaped micropores. Kernels 5 and 6 are designed for materials, in which the mesopore system is comprised of large cage-like pores connected by smaller mesopores and/or embedded in microporous matrix, such as carbons prepared from 3D colloidal templates, like 3DOm [13]. In these materials, the isotherm typically has H2 hysteresis type, indicating pronounced pore blocking effects. The pore size analysis in this situation should be based on the adsorption branch. While we do not consider any other adsorbates here, the schemes for compilation of kernels suggested above could be used for compiling kernels for other adsorbates, e.g. argon.

The choice of the kernel for deriving the PSD for a given carbon sample should be made based on the *a priori* information about the adsorbent material. Synthesis and/or templating procedure determines the shape of the mesopores (channel-like vs. cage-like structure) to use cylindrical or spherical kernel, respectively. The model for micropores (channels or slit-pores) should be chosen based on degree of activation. Another criterion for the choice of a certain DFT kernel is the fitting of resulting PSD to the experimental isotherm (Section 4). Improper choice of pore geometry usually leads to bad fitting results.

4. Application examples

Adsorption experiments on 3DOm and CMK-3 carbons have been performed with a Quantachrome Autosorb iQ MP and Quantachome Autosorb 1 MP instruments. Prior to the analysis the samples were outgassed at 423 K under turbomolecular pump vacuum.

4.1. *CMK-3 carbons*

CMK-3 carbons [12] are the inverse replicas of two-dimensional ordered mesoporous silicas of type SBA-15. The carbon skeleton of CMK-3 represents a network of aligned cylindrical rods connected by crossbars. Although, the mesopores between these rods have a complex shape, a model of cylindrical channels is typically assumed for characterization purposes [24]. In addition to the main mesoscopic channels, CMK-3 skeleton is microporous.

A high resolution nitrogen (77.4 K) adsorption/desorption isotherm was measured on a CMK-3 sample which is presented in Fig. 2a. We applied the QSDFT cylindrical equilibrium and cylindrical adsorption kernels (kernels 1 and 2) to obtain the pore size distributions (Fig. 2b). The fitting of the experimental isotherm using QSDFT kernels, i.e. convolution of obtained PSD with QSDFT kernels isotherms (r.h.s. of Eq. (8)) is given in Fig. 2a (plotted linearly, to illustrate the good fit in the pressure range of hysteresis) for both adsorption and desorption branches. The fitting of the experimental isotherm, plotted logarithmically to highlight the fit in the low pressure region, is given for the QSDFT cylindrical kernel in Fig. 2b. Finally, the comparison of pore size distributions obtained using QSDFT cylindrical adsorption kernel, cylindrical equilibrium kernel (kernel 1) and NLDFT cylindrical equilibrium kernel is given in Fig. 2c.

CMK-3 pore size distributions calculated from the QSDFT cylindrical adsorption kernel 2 (applied on the adsorption branch of the isotherm) and equilibrium kernel 1 (applied on the desorption branch of the isotherm) give two distinguished peaks – one in the mesopore range, at 4.7–4.8 nm and another in the micropore range around 1 nm (Fig. 2c). The overlap of the pore size distributions indicates that the

Author's personal copy

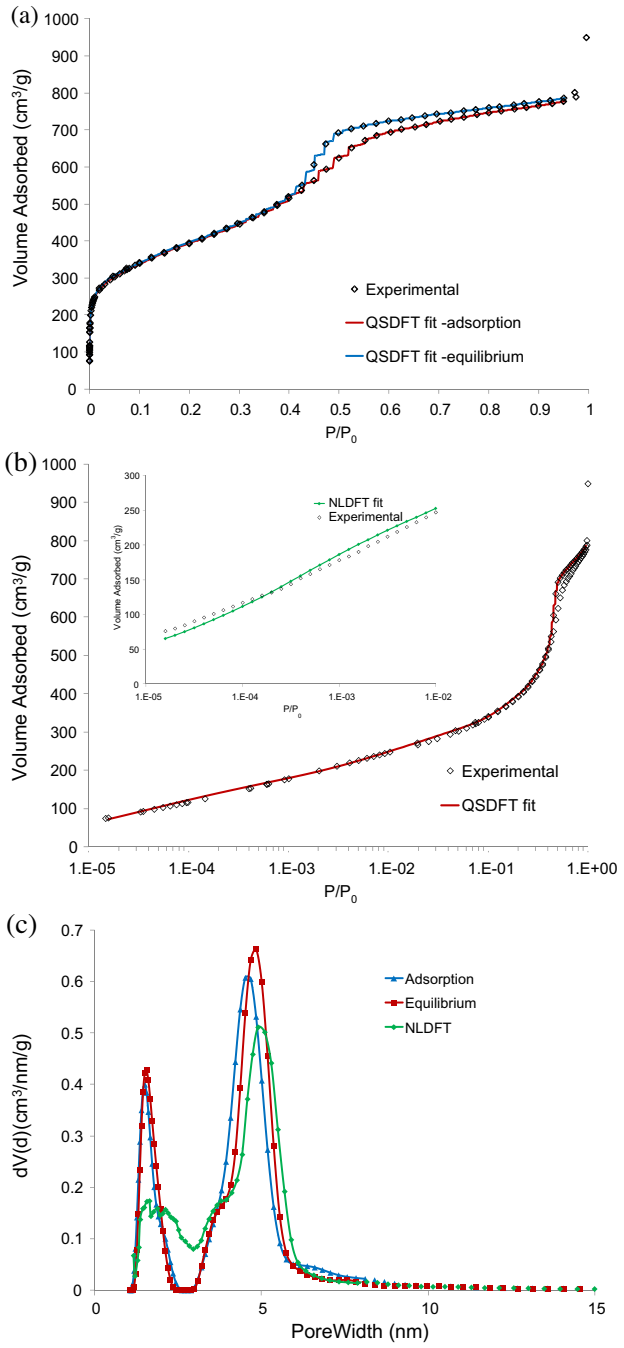

Fig. 2 – Nitrogen (77.4 K) adsorption on CMK-3 sample. (a) Experimental isotherm with fit from QSDFT cylindrical adsorption (kernel 2) and cylindrical equilibrium (kernel 1) kernels (b) experimental isotherm and fit from QSDFT cylindrical equilibrium kernel (plotted semi-logarithmically), inset – fit from NLDFT equilibrium kernel and (c) pore size distributions from QSDFT cylindrical adsorption and cylindrical equilibrium kernels derived from adsorption and desorption branches of experimental isotherms and from NLDFT cylindrical pore equilibrium kernel.

position of the desorption branch of the isotherm is not strongly affected by pore blocking effects, i.e. desorption occurs close to the equilibrium transition and the hysteresis in this CMK-3 sample is mainly caused by so-called delayed condensation. Fig. 2a confirms very good agreement between the calculated QSDFT isotherms for both the adsorption branch (adsorption kernel) and desorption (equilibrium kernel) with the experimental data.

In addition to DFT, we also applied a geometrical model of hexagonally arranged carbon rods of Joo et al. [24] and XRD data for this sample to calculate the mesopore size by means of the following equation:

$$w_{CMK-3} = d_{100}\left[\frac{4}{3} - c\left(\frac{1/\rho + V_{mi}}{V_p + 1/\rho + V_{mi}}\right)^{1/2}\right]. \quad (8)$$

The total pore volume was calculated using the Gurvich rule at $P/P_0 = 0.6$ after the pore condensation into the primary CMK-3 mesopores and the micropore volume (V_{mi}) was calculated using the *t*-plot method. The mesopore volume (V_p) was calculated by subtracting the micropore volume from the total pore volume. The mass density of the carbon, ρ, was taken as 2.05 g/cm^3 and c, which is a constant characteristic of pore geometry, is equal to 1.213 for cylindrical pores. The obtained QSDFT pore size (4.7 nm calculated from the adsorption branch and 4.8 nm calculated from the desorption branch) agrees well with the pore size derived from XRD (5.0 nm), confirming that the QSDFT method accurately calculates the pore size from the experimental data.

The pore size distribution derived from the NLDFT equilibrium kernel (applied on the desorption branch of the isotherm) is also shown in Fig. 2c. Although the peaks on both PSDs in the micropore and mesopore regions are located at roughly the same positions, QSDFT does not show any pores between these peaks. This difference is likely a consequence of the approximation of the smooth experimental isotherm with the NLDFT isotherms with layering steps.

PSD calculation depends on the type of the hysteresis loop, which is also affected by the pore network morphology. The nitrogen (77.4 K) isotherm on another CMK-3 carbon sample is presented in Fig. 3a. In this sample as compared to the previous one (Fig. 2a), the hysteresis loop has some characteristics of type H2 (according to the IUPAC classification). It indicates the possibility of pore blocking affecting the pressure where pore evaporation/desorption occurs. Therefore, for this sample an accurate PSD is calculated from the adsorption branch of the isotherm (where pore blocking effects are not present) using the QSDFT cylindrical adsorption kernel (kernel 2) which takes correctly into account the delay in pore condensation due to metastable pore fluid. In contrast, for this sample the pore size distribution obtained from the desorption branch of the isotherm (using kernel 1) noticeably deviates from that of the adsorption branch and gives an incorrect pore size distribution because this kernel assumes that desorption occurs via equilibrium evaporation from the pore, which is not the case for this CMK-3 sample. These pore size distributions are shown in Fig. 3b and the fit for kernel 2 is shown on the isotherm in Fig. 3a.

4.1.1. *3DOm carbons*

To test the QSDFT kernels for cage-like mesopore systems, we studied the 3-dimensionally-ordered mesoporous (3DOm) carbon samples described in [13]. These carbons were obtained by templating three-dimensional colloidal crystals

Author's personal copy

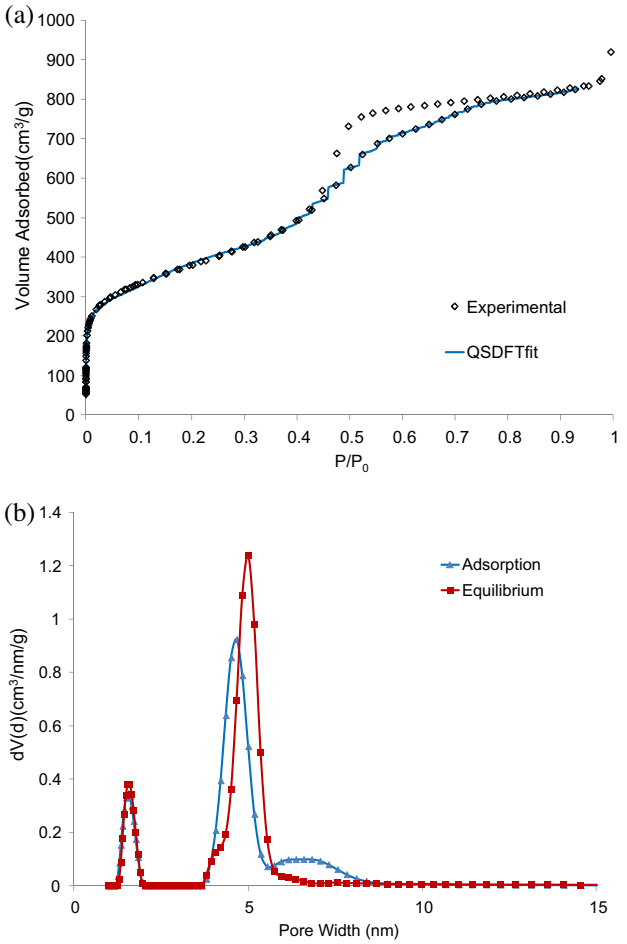

Fig. 3 – Nitrogen (77.4 K) adsorption on an additional CMK-3 sample. (a) Experimental isotherm with fit from QSDFT cylindrical adsorption kernel (kernel 2) and (b) pore size distributions from QSDFT cylindrical adsorption kernel and equilibrium kernels (kernels 2 and 1).

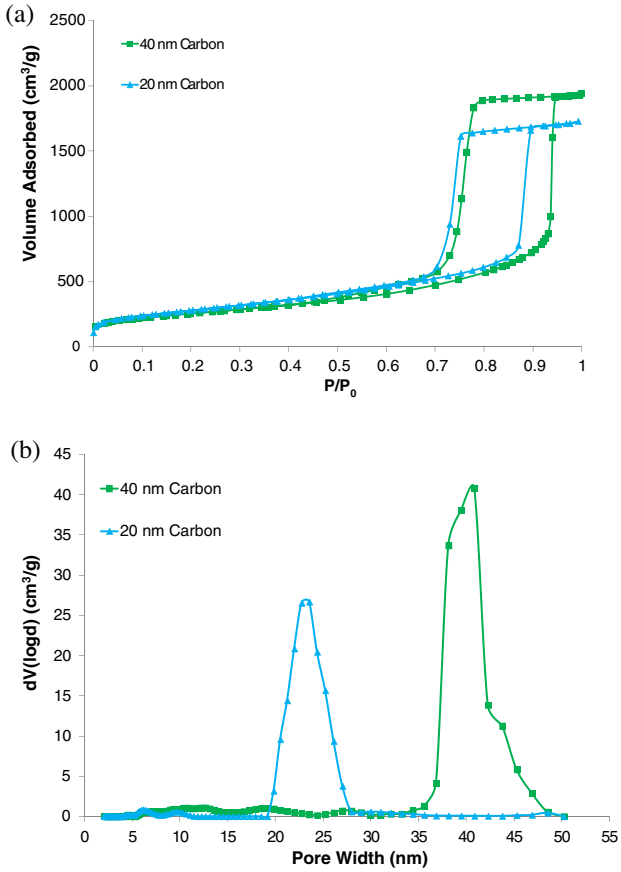

Fig. 4 – Nitrogen (77.4 K) adsorption data from [13]. (a) Experimental isotherms and (b) pore size distributions calculated using the QSDFT cylindrical/spherical adsorption kernel (kernel 5).

formed from lysine-silica nanoparticles. Use of colloidal crystals with various primary particle sizes allows one to tailor the pore size of 3DOm carbons. First, we considered the nitrogen adsorption data measured on two samples from [13], obtained from colloid particles with sizes of ca. 20 and 40 nm (Fig. 4a). For the characterization of the large mesopores obtained by templating the spherical pore geometry should be used, while for smaller mesopores and micropores (if present), which are not related to the templating, the cylindrical and/or slit pore geometry could be assumed.

In materials with spherical pores, desorption/evaporation is always affected by either pore blocking [25] or cavitation [26] effects. Hence the pore size of the main cavity can only be obtained from the adsorption branch by applying a dedicated QSDFT kernel (cylindrical–spherical), which correctly takes into account the delay in condensation in spherical carbon pores. The nitrogen (77.4 K) isotherms for the two 3DOm carbon samples templated using 20 and 40 nm particles are shown in Fig. 4a. Additionally, the desorption branches of these two carbons nearly coincide, indicating that these two materials consist of pores with similar opening sizes. The pore structure is being further investigated using hysteresis scanning experiments.[2] The pore size distributions for these two samples obtained using kernel 5 (shown in Fig. 4b) have pronounced peaks at 23.6 and 40.9 nm for "20 nm" and "40 nm" samples, respectively. The pore sizes match closely with the pore sizes observed for these materials using SEM [13], confirming the accuracy of the QSDFT kernels.

The verified cylindrical-spherical adsorption kernel (5) was then used to determine the pore size distribution of two new, additional 3DOm carbon samples templated using 10 and 30 nm nanoparticles. First, high resolution nitrogen (77.4 K) isotherms were measured over the full micro- and mesopore range (unlike in the previous samples which were not measured down to very low pressures) and are shown in Fig. 5a. QSDFT cylindrical-spherical adsorption kernel was used to plot the pore size distributions shown in Fig. 5b. The peaks in the pore size distributions match closely with the pore sizes expected from the templating particles. Additionally, the

[2] Cychosz KA, Guo X, Gor GY, Fan W, Neimark AV, Tsapatsis M, Thommes M. Characterization of carbons with ordered spherical mesopores by high resolution sorption and hysteresis scanning experiments in combination with novel QSDFT methods, manuscript in preparation.

Author's personal copy

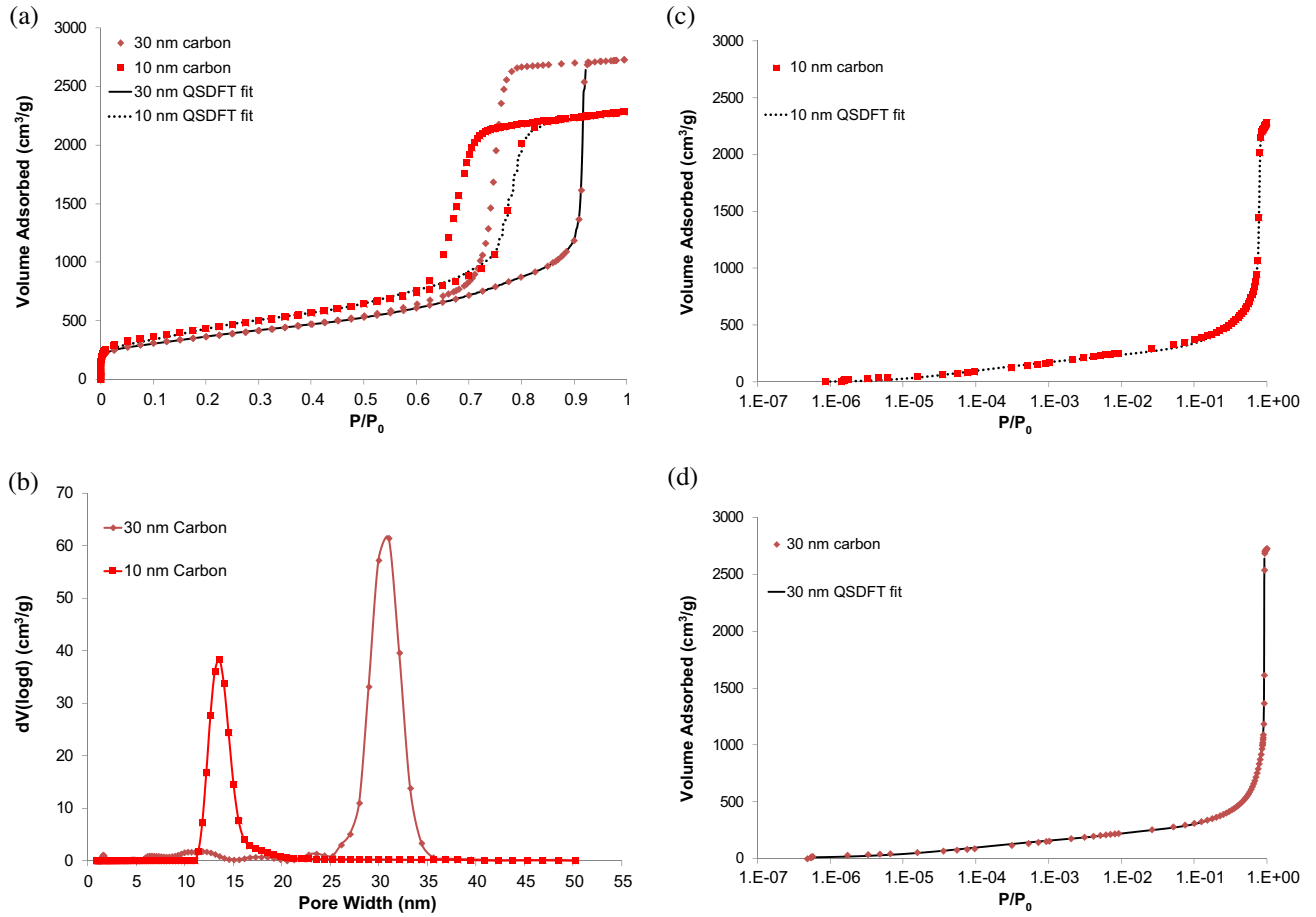

Fig. 5 – Nitrogen (77.4 K) adsorption on 3DOm samples templated from 10 and 30 nm particles. (a) Experimental isotherms with QSDFT fits from the cylindrical–spherical adsorption kernel (kernel 5); (b) pore size distributions from QSDFT cylindrical–spherical adsorption kernel derived from adsorption branch of experimental isotherms; (c) and (d) experimental isotherms and fits from QSDFT cylindrical–spherical adsorption kernel (plotted semi-logarithmically) for 10 and 30 nm samples correspondingly.

QSDFT fits are shown with the isotherms in Fig. 5a, and good agreement is found, i.e. the QSDFT kernels are able to predict the delay in condensation of the adsorption branch of spherical pore carbons. Logarithmic plots of the isotherms with the QSDFT fits are given in Fig. 5c and d. Not only are the kernels able to predict the adsorption branch of the hysteresis loop, but they are also capable of accurately predicting the pore size distribution in the full micro- and mesopore range and confirm that the microporosity in these samples is negligible.

5. Conclusions

We propose a new QSDFT method for characterization of micro–mesoporous carbons using nitrogen (77.4 K) adsorption. The method takes into account the geometries of the pores, solid–fluid interactions and surface roughness specific for carbons. Since the roughness of the surface is taken into account, the QSDFT isotherms do not display artificial layering steps characteristic to NLDFT calculations. Six kernels of theoretical QSDFT isotherms were constructed for PSD calculations from adsorption isotherms with different types of the hysteresis loop reflecting different morphologies in micro–mesoporous carbons of cage-like and channel-like pore geometries. These kernels embrace the whole range of micro- and mesopores, from 0.4 to 50 nm, which can be probed by nitrogen adsorption. The roughness parameter used in QSDFT calculations corresponded to the reference nitrogen isotherm on Cabot carbon chosen as the reference adsorbent [11].

The new QSDFT methods for cylindrical and spherical mesopore geometries have been validated using XRD and SEM data on CMK-3 and 3DOm carbons, respectively and have been applied to additional ordered carbon samples. Our results clearly demonstrate the applicability of the QSDFT methods for reliable pore size and pore volume analyses of micro–mesoporous carbon materials. As such, the current work extends the QSDFT method, initially suggested to PSD analysis of disordered carbons based on the slit-shape pore model [11], to the ordered and hierarchical micro–mesoporous carbons prepared via various templating techniques, such as CMK-3 and CMK-5, 3DOm, FDU-14, FDU-15, and FDU-16 [27–29].

Acknowledgements

The authors thank Michael Fröba and Michael Tsapatsis for providing 3DOm and CMK-3 samples and additional data;

Author's personal copy

Peter Ravikovitch and Yangzheng Lin for multiple illuminating discussions and help with the QSDFT code. AVN acknowledges partial support from the NSF ERC "Structured Organic Particulate Systems".

REFERENCES

[1] Neimark AV, Ravikovitch PI, Vishnyakov A. Bridging scales from molecular simulations to classical thermodynamics: density functional theory of capillary condensation in nanopores. J Phys-Condens Mater 2003;15(3):347–65.
[2] Neimark AV, Ravikovitch PI, Vishnyakov A. Inside the hysteresis loop: multiplicity of internal states in confined fluids. Phys Rev E 2002;65(3):031505.
[3] Ravikovitch PI, Neimark AV. Density functional theory model of adsorption on amorphous and microporous silica materials. Langmuir 2006;22(26):11171–9.
[4] Ravikovitch PI, Vishnyakov A, Russo R, Neimark AV. Unified approach to pore size characterization of microporous carbonaceous materials from N_2, Ar, and CO_2 adsorption isotherms. Langmuir 2000;16(5):2311–20.
[5] Neimark AV, Ravikovitch PI, Grun M, Schuth F, Unger KK. Pore size analysis of MCM-41 type adsorbents by means of nitrogen and argon adsorption. J Colloid Interface Sci 1998;207(1):159–69.
[6] Ravikovitch PI, Neimark AV. Density functional theory of adsorption in spherical cavities and pore size characterization of templated nanoporous silicas with cubic and three-dimensional hexagonal structures. Langmuir 2002;18(5):1550–60.
[7] Thommes M, Smarsly B, Groenewolt M, Ravikovitch PI, Neimark AV. Adsorption hysteresis of nitrogen and argon in pore networks and characterization of novel micro- and mesoporous silicas. Langmuir 2006;22(2):756–64.
[8] Thommes M. Physical adsorption characterization of nanoporous materials. Chem Ing Tech 2010;82(7):1059–73.
[9] Thommes M. Textural characterization of zeolite and ordered mesoporous materials by physical adsorption. 3rd ed. Elsevier; 2007.
[10] ISO-15901-3. Pore size distribution and porosity of solid materials by mercury porosimetry and gas adsorption. Analysis of micropores by gas adsorption, 2007.
[11] Neimark AV, Lin Y, Ravikovitch PI, Thommes M. Quenched solid density functional theory and pore size analysis of micro–mesoporous carbons. Carbon 2009;47(7):1617–28.
[12] Jun S, Joo SH, Ryoo R, Kruk M, Jaroniec M, Liu Z, et al. Synthesis of new, nanoporous carbon with hexagonally ordered mesostructure. J Am Chem Soc 2000;122(43):10712–3.
[13] Fan W, Snyder MA, Kumar S, Lee P-S, Yoo WC, McCormick AV, et al. Hierarchical nanofabrication of microporous crystals with ordered mesoporosity. Nat Mater 2008;7(12):984–91.
[14] Neimark AV, Ravikovitch PI. Capillary condensation in MMS and pore structure characterization. Micropor Mesopor Mater 2001;44:697–707.
[15] Lastoskie C, Gubbins KE, Quirke N. Pore-size distribution analysis of microporous carbons – a density-functional theory approach. J Phys Chem-USA 1993;97(18):4786–96.
[16] Ravikovitch PI, O'Domhnaill SC, Neimark AV, Schuth F, Unger KK. Capillary hysteresis in nanopores: theoretical and experimental studies of nitrogen adsorption on MCM-41. Langmuir 1995;11(12):4765–72.
[17] Gubbins KE, Liu YC, Moore JD, Palmer JC. The role of molecular modeling in confined systems: impact and prospects. Phys Chem Chem Phys 2011;13(1):58–85.
[18] Rosenfeld Y. Free-energy model for the inhomogeneous hard-sphere fluid mixture and density-functional theory of freezing. Phys Rev Lett 1989;63(9):980–3.
[19] Rosenfeld Y, Schmidt M, Löautwen H, Tarazona P. Fundamental-measure free-energy density functional for hard spheres: dimensional crossover and freezing. Phys Rev E 1997;55(4):4245–63.
[20] Ravikovitch PI. Characterization of nanoporous materials by gas adsorption and density functional theory. PhD Thesis. Yale University, 1998.
[21] Lawson CL, Hanson RJ. Solving least squares problems. Philadelphia: SIAM; 1995.
[22] Joo SH, Choi SJ, Oh I, Kwak J, Liu Z, Terasaki O, et al. Ordered nanoporous arrays of carbon supporting high dispersions of platinum nanoparticles. Nature 2001;412(6843):169–72.
[23] Sang LC, Vinu A, Coppens MO. Ordered mesoporous carbon with tunable, unusually large pore size and well-controlled particle morphology. J Mater Chem 2011;21(20):7410–7.
[24] Joo SH, Ryoo R, Kruk M, Jaroniec M. Evidence for general nature of pore interconnectivity in 2-dimensional hexagonal mesoporous silicas prepared using block copolymer templates. J Phys Chem B 2002;106(18):4640–6.
[25] Vishnyakov A, Neimark AV. Monte Carlo simulation test of pore blocking effects. Langmuir 2003;19(8):3240–7.
[26] Rasmussen CJ, Vishnyakov A, Thommes M, Smarsly BM, Kleitz F, Neimark AV. Cavitation in metastable liquid nitrogen confined to nanoscale pores. Langmuir 2010;26(12):10147–57.
[27] Meng Y, Gu D, Zhang F, Shi Y, Cheng L, Feng D, et al. A family of highly ordered mesoporous polymer resin and carbon structures from organic–organic self-assembly. Chem Mater 2006;18(18):4447–64.
[28] Zhang F, Meng Y, Gu D, Yan, Yu C, Tu B, et al. A facile aqueous route to synthesize highly ordered mesoporous polymers and carbon frameworks with Ia3d bicontinuous cubic structure. J Am Chem Soc 2005;127(39):13508–9.
[29] Meng Y, Gu D, Zhang FQ, Shi YF, Yang HF, Li Z, et al. Ordered mesoporous polymers and homologous carbon frameworks: amphiphillic surfactant templating and direct transformation. Angew Chem-Int Ed 2005;44(43):7053–9.